Vacuum-ultraviolet photoreduction of graphene oxide: Electrical conductivity of entirely reduced single sheets and reduced micro line patterns

AUTHOR(S):

Tu, Yudi; Ichii, Takashi; Utsunomiya, Toru; Sugimura, Hiroyuki

CITATION:

Tu, Yudi ...[et al]. Vacuum-ultraviolet photoreduction of graphene oxide: Electrical conductivity of entirely reduced single sheets and reduced micro line patterns. Applied Physics Letters 2015, 106(13): 133105.

ISSUE DATE:

2015-04-01

URL:

http://hdl.handle.net/2433/198886

AIP | Applied Physics Letters

Vacuum-ultraviolet photoreduction of graphene oxide: Electrical conductivity of entirely reduced single sheets and reduced micro line patterns

Yudi Tu, Takashi Ichii, Toru Utsunomiya, and Hiroyuki Sugimura

Citation: Applied Physics Letters **106**, 133105 (2015); doi: 10.1063/1.4916813
View online: http://dx.doi.org/10.1063/1.4916813
View Table of Contents: http://scitation.aip.org/content/aip/journal/apl/106/13?ver=pdfcov
Published by the AIP Publishing

APPLIED PHYSICS LETTERS **106**, 133105 (2015)

Vacuum-ultraviolet photoreduction of graphene oxide: Electrical conductivity of entirely reduced single sheets and reduced micro line patterns

Yudi Tu, Takashi Ichii, Toru Utsunomiya, and Hiroyuki Sugimura[a)]
Department of Materials Science and Engineering, Graduate School of Engineering, Kyoto University, Kyoto 606-8501, Japan

(Received 16 January 2015; accepted 16 March 2015; published online 1 April 2015)

We here report a scanning probe method to locally and directly research the electrical properties of vacuum-ultraviolet (VUV) reduced graphene oxide. The measured electrical conductivity of individual VUV-reduced GO (VUV-rGO) sheets by using conductive atomic force microscopy (CAFM) reached 0.20 $S \cdot m^{-1}$ after 64 min irradiation, which was clearly enhanced compared with the pristine GO. According to the X-ray photoelectron spectroscopy results, the recovered conductivity of VUV-rGO could be ascribed to the partial elimination of oxygen-containing functional groups and the rapid reconstruction of the C=C bonds. Heterogeneously distributed low- and high-conductivity domains (with a diameter of tens of nanometer to ca. 500 nm) were found from current mapping of the VUV-rGO sheet. By applying photomask lithography, rGO regions were drawn into single GO sheet and were researched by CAFM. The in-plane lateral conductivity of rGO regions increased obviously compared with pristine GO regions. © *2015 AIP Publishing LLC*.
[http://dx.doi.org/10.1063/1.4916813]

During the last decade, two-dimensional (2D) materials have drawn tremendous attention among materials researchers because of their outstanding performance throughout the material scientific fields. As the origin of this fashion, graphene, a single layer of carbon atoms with a honeycomb structure, is perceived as the next-generation material to replace the role of silicon in electronics. Owing to its nearly infinite π-conjugated system, graphene shows incredibly high electrical conductivity, which is one of its most important characteristics. Nonetheless, the low yield of high-quality graphene by mechanical cleavage is not as impressive as its fantastic electrical properties. To solve this problem, a graphene derivative, i.e., reduced graphene oxide (rGO), was developed. Based on the previous reports, rGO can be derived massively from chemically oxidized graphite (i.e., graphene oxide, GO) by applying various reduction processes. It was found that GO has heterogeneous structures combining both conductive graphitic domains and defective domains.[1–3] The defective domains contain distortions and oxygen-containing functional groups (OFGs, e.g., hydroxyl groups, carbonyl groups, carboxyl groups, etc.) and their local decorations make GO an insulator. It has been widely reported that thermal or chemical reduction can reduce GO to a relatively high degree.[4] After thermal or chemical reduction, the π-conjugated system can be partially reconstructed by OFG elimination and graphitic domain reconnection. However, the residual OFGs and sp^3 domains derived from eliminated OFGs still possess a great part of the rGO basal plane and affect the electrical conductivity of rGO. Therefore, the microstructures of GO and rGO have been deeply studied globally and atomically by applying both spectroscopic and microscopic methods. Raman spectroscopy is a typical non-destructive method for investigating graphene-like materials and has been thoroughly used for quantifying the defective domain size of GO.[1] Microscopic methods, such as scanning tunneling microscopy (STM) and transmission electron microscopy (TEM), gave in-depth information of the GO and rGO local structures at the atomic level.[2,3,5] Electrostatic force microscopy (EFM) was also utilized to record domain evolution during the GO reduction process by detecting the difference of the electrostatic force from GO to rGO.[6] Another powerful micro/nano scanning probe method, conductive atomic force microscopy (CAFM), has been developed to research the electrical properties of carbon nanotubes,[7] nanowires,[8] quantum dots,[9] metal-molecule-metal junctions,[10,11] etc., providing a detailed correlation between structural and electrical characteristics. Inspired by the former studies, CAFM has also been reported to have some successful applications in characterizing chemically or photochemically reduced rGO.[12,13]

Although thermal and chemical reduction are effective and are easily realized in the laboratory, industrial manufacturers would not be satisfied with the high temperatures and toxic reduction processes applied in thermal and chemical reduction. To overcome these drawbacks and to combine reduction with a simultaneous patterning process, we have demonstrated a high-efficiency reduction induced by vacuum-ultraviolet (VUV) light irradiation and have further applied it to resist-free photolithography of the rGO/GO pattern, as schematically illustrated in Figure 1(a).[14] For instance, a periodic pattern of 500 nm rGO lines with 2.5 μm pitches was drawn into a micrometer-scale GO sheet. As we have reported, the highest resolution of this patterning method was the 500 nm rGO lines with a pitch of 1500 nm.[14] However, this is not the absolute limit of the VUV patterning method, since our group has achieved more minute patterning nearly 200 nm using the same VUV light and an alumina nanohole mask.[15] The AFM topography and corresponding Kelvin-probe force microscopic (KFM) surface potential

[a)]E-mail: sugimura.hiroyuki.7m@kyoto-u.ac.jp. Tel.: +81-75-753-9131

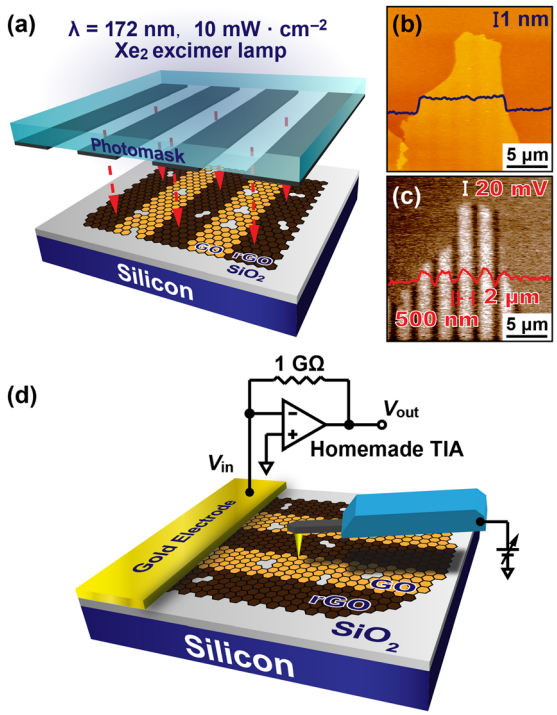

FIG. 1. (a) Illustration of the VUV patterning process. (b) AFM topography of a patterned single-layer GO sheet and (c) a corresponding KFM surface potential image to (b). (d) Illustration of the CAFM apparatus.

distribution of the patterned sheet are shown in Figures 1(b) and 1(c). However, the electrical conductivity and the micro electrical structures of rGO and rGO/GO pattern have not been clearly investigated yet. Their clarification will be a crucial step toward understanding and application of this kind of rGO.

Here, we demonstrate a CAFM measurement associated with X-ray photoelectron spectroscopy (XPS) study for clarifying the electrical conductivity and the domain distribution in VUV-reduced GO (VUV-rGO) and patterned rGO/GO sheets. CAFM measurements of an individual single-layer rGO sheet demonstrated the recovery of electrical conductivity owing to the elimination of OFGs and the rapid reconstruction of the C=C bonds. The high-resolution current mapping revealed that the low-conductivity domains were randomly distributed with a diameter of tens to several hundred nanometers and were enclosed by the high-conductivity domains in the VUV-rGO sheet. A patterned rGO/GO sheet was prepared by submitting an as-prepared large-area single-layer GO sheet to VUV irradiation through a photomask. Current mapping of the patterned rGO/GO sheet showed that the electrical conductivity of rGO regions clearly increased compared with the GO regions.

GO sheets with a large size of 20–50 μm were prepared through a modified Hummers' method.[16] Elemental analysis of the as-prepared GO was conducted on an XPS to ensure that all impurities possibly induced by synthesis (e.g., Mn-containing ions, Na^+, K^+, NO_3^-, and SO_4^{2-}, etc.) were removed. The VUV-rGO was prepared by irradiating VUV light on the single-layer GO sheet for 64 min. A typical experiment started from the spin coating of GO aqueous solution onto a carefully cleaned and hydrophilically modified highly p-doped silicon (with 90 nm silicon dioxide) substrate. The substrate was then set into the high vacuum chamber ($<10^{-3}$ Pa) and irradiated by VUV light (Xe excimer lamp, 172 nm, 10 mW·cm^{-2}) for 64 min. The patterned rGO/GO sheets were fabricated by irradiating VUV light on single-layer GO sheet via a photomask (100 nm thick Cr patterns on a 2 mm thick quartz plate −93% transparency at 172 nm, as shown in Figure 1(a)) for 2 min under the same conditions described above. XPS elemental analyses of pristine GO, 2-min irradiated GO (rGO_2) and 64-min irradiated GO (rGO_{64}), were performed to investigate the correlation between the electrical properties and elemental components. CAFM measurements were performed on an Asylum MFP-3D AFM (Oxford Instruments) to measure the electrical conductivity of the VUV-rGO sheet and patterned rGO/GO sheets, as shown in Figure 1(d). Before the electrical measurement, a Ti/Au electrode (10 nm for each, Ti layer act as an adhesion layer) was deposited onto reduced or patterned GO sheets through a shadow mask to form an electrical contact. A homemade I−V transimpedance amplifier (TIA, with a 1 GΩ feedback resistor) was used to amplify the current signal and an Rh-coated Si cantilever [SI-DF3-R (100 nm Rh coated), 1.6 N/m, 23 kHz, Hitachi Hi-tech Co. Ltd.] was used as a local electrode for mapping the local current from reduced or patterned GO sheets with a maintained load of ca. 17.5 nN. The topographic images were taken simultaneously in contact mode. A built-in optical microscope assisted in the locating of rGO sheet. The tip bias was set between − 3 V and 0 V to ensure that no redox reactions happened on the GO or rGO sheet.[12] All the measurements were performed at ambient environment (15–25 °C with a relative humidity of 30%–40%). For studying the recovery of π-conjugated system and the distribution of domains in GO and rGO, the micro Raman spectroscopy was performed. The measurements were conducted on the rGO and the GO region of a patterned rGO/GO pattern by using a Horiba XploRA Raman microscope with a 532 nm line laser as the excitation source.

As we previously reported,[14] the VUV reduction saturated after 64 min of irradiation. We carried out the current mapping in rGO_{64} in order to demonstrate the highest electrical conductivity of the VUV-rGO. Analysis by XPS was also performed to demonstrate the reconstruction of C=C bonds, which was linked to the restoration of the π-conjugated system. The C1s core-level XPS spectra of GO and rGO_{64} are shown in Figure 2(a). All of the spectra were calibrated to the Si 2p (SiO_2) peak at 103.5 eV and normalized to the intensity of the C 1s main peak. To better understand the details of OFG evolution, the spectra were further deconvoluted to 6 peaks,[17] i.e., sp^2 C=C [at 284.4 eV with full width half maximum (FWHM) of 1.50 eV], sp^3 C-C (at 285.0 eV with FWHM of 1.36 eV), C-OH (at 286.2 eV, with FWHM of 1.46 eV), C-O-C (at 286.9 eV, with FWHM of 1.24 eV), C=O (at 287.9 eV, with FWHM of 1.57 eV), and COOH (at 289.1 eV, with FWHM of 1.41 eV). The percentages of each peak (referred to $P_{C=C}$, P_{C-C}, P_{C-OH}, P_{C-O-C}, $P_{C=O}$, and P_{COOH}) were calculated by the accessorial software and used for calculating the oxygen carbon atomic ratio, $R_{O/C}$, through the following equation:

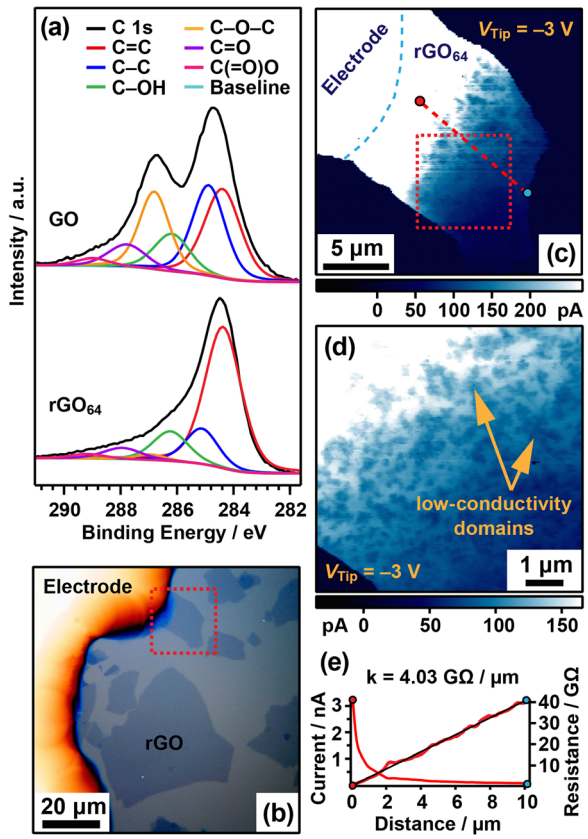

FIG. 2. (a) XPS C1s spectra of pristine GO and rGO_{64}. (b) An optical microscopic image of Ti/Au electrode and rGO_{64} sheets. The sheet in the red dashed frame was electrically connected to Ti/Au electrode. (c) CAFM current mapping corresponding to the rGO sheet shown in the red dashed frame in (b) with a tip bias of − 3 V. (d) A zoom-in current mapping of the rGO sheet in the dashed frame in (c). The low-conductivity domains are clearly revealed. (e) Current profile and corresponding resistance profile of the red dashed line shown in (c). The current distribution showed reciprocal proportion to the distance from the electrode.

$$R_{O/C} = \frac{P_{C\text{–}OH} + \frac{1}{2}P_{C\text{–}O\text{–}C} + P_{C=O} + 2P_{COOH}}{P_{C=C} + P_{C\text{–}C} + P_{C\text{–}OH} + P_{C\text{–}O\text{–}C} + P_{C=O} + P_{COOH}}. \quad (1)$$

After VUV irradiation, the peak percentages of OFGs decreased with $R_{O/C}$ declining from 0.36 to 0.25, which indicated that OFGs were partially removed. In detail, $P_{C\text{–}O\text{–}C}$ decreased from 20.1% to 3.0%, $P_{C\text{–}C}$ decreased from 27.7% to 11.0%, $P_{C=O}$ decreased from 9.3% to 5.8%, and $P_{C=C}$ increased from 28.7% to 65.0%. Meanwhile, $P_{C\text{–}OH}$ and P_{COOH} showed no obvious change, their values being ∼12.0% and ∼2.5%, respectively. These dramatic changes indicate possible recovery of higher electrical conductivity. Matsumoto *et al.* have reported electrical conductivity of rGO vertical to its basal plane on a conductive substrate.[13] However, vertical electrical conductivity cannot demonstrate the real capability of rGO to transport current because the current flows in a lateral direction on the rGO basal plane when rGO is used as a transparent electrode or as the conductive channel in a transistor. And, as we mentioned before, the heterogeneous distribution of graphitic and defective domains will result in an uncertainty of electrical conductivity vertical to the sheet plane. Therefore, we applied CAFM to measure the lateral electrical conductivity. As to be a facile method to image graphene-related nanosheets,[18] an optical microscope was used to locate one rGO_{64} sheet that was electrically contacted to the Ti/Au electrode, as shown in the red dashed frame in Figure 2(b). The corresponding CAFM current mapping image of the rGO_{64} sheet as shown in Figure 2(c) demonstrates an obvious electrical conductivity. A zoom-in current mapping of rGO_{64} was shown in Figure 2(d), corresponding to the red dashed frame in Figure 2(c). A number of low-conductivity domains are found to be randomly distributed in the rGO sheet. The size of these low-conductivity domains ranges from several tens to hundreds of nanometers. The current profile and the corresponding calculated resistance profile (shown in Figure 2(e)) of the red dashed line in Figure 2(c) show that the current and resistance are reciprocally proportional and directly proportional to the distance from the Ti/Au electrode, respectively, which matches the classic Ohm's law, i.e., $U = IR$. The slope of resistance-distance was calculated to be 4.03 $G\Omega \cdot \mu m^{-1}$ from a linear fitting. Because the current pathway is 2D, the electrical conductivity was calculated by assuming that only the triangle region of rGO formed by the tip and the electrode edge act as the conductive channel. The contact area of the tip and rGO was estimated to be 12.6 nm^2 by applying the Hertzian contact mechanics model.[12] The approximate electrical conductivity was estimated to be ca. 0.20 $S \cdot m^{-1}$. Sow *et al.* reported a laser-induced thermal reduction on GO under inert atmosphere and the measured electrical conductivity of multi-layered rGO was 1.1 $S \cdot m^{-1}$.[19] Zhang *et al.* also reported the photo-reduction of the ca. 50-layered GO thin film by using a femtosecond laser. The fabricated rGO film showed the electrical conductivity of 2.56×10^4 $S \cdot m^{-1}$.[20] It should be noted that we here measured the rGO single layer attached to the substrate. Unlike the multi-layered rGO that have the capability to transport the carriers between different layers, the single-layered rGO can only transport carrier within the single basal plane and affected by the underlying substrate. What is more important is that because the CAFM applied a nano-scaled probe electrode, the defects near the probe would highly affect the electrical conductivity. Therefore, it is difficult to directly compare the electrical conductivity of VUV-rGO with the reported values.

As the most important advantage of VUV induced reduction, the capability to draw rGO regions into a GO sheet is demonstrated here. The CAFM current mapping of the rGO/GO pattern is shown in Figure 3. A periodic pattern of 5 μm GO and 5 μm rGO lines was drawn by the VUV photolithography. The reflection of VUV light from the interface between Si and SiO_2 would cause the pattern to lose some precision. Hence, the sheet was irradiated and patterned for only 2 min. Further research is needed here, too. The XPS C1s spectra of rGO_2 (Figure 3(a)) showed that after 2 min VUV irradiation, $P_{C\text{-}O\text{-}C}$ decreased from 20.1% to 6.8%, $P_{C\text{-}C}$ decreased from 27.7% to 10.5%, and $P_{C=C}$ increased from 28.7% to 51.5% though the $R_{O/C}$ with the value of ca. 0.36 showed no obvious change. This dramatic change happened within only 2 min while the VUV light intensity was only 10 $mW \cdot cm^{-2}$, which indicates that VUV reduction is fast and effective. Because the electrical conductivity of graphene-like

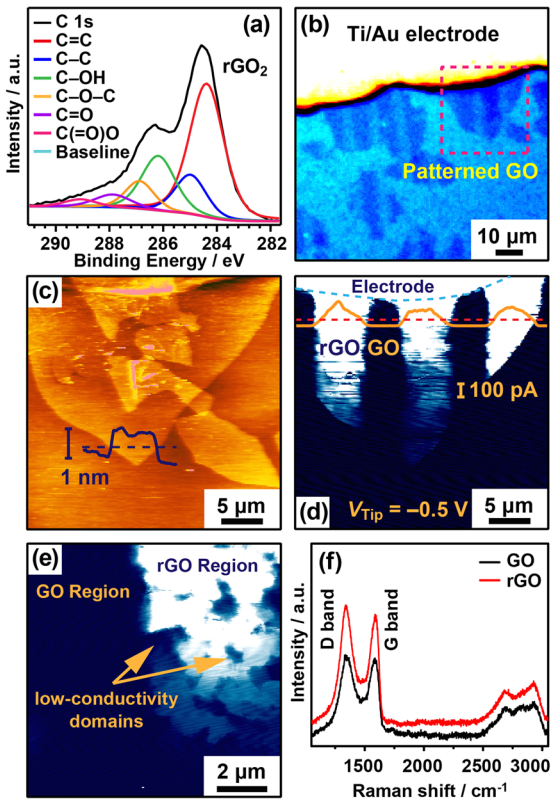

FIG. 3. (a) XPS spectra of rGO_2. (b) An optical microscopic image of Ti/Au electrode and patterned sheets (periodic pattern of 5 μm GO and 5 μm rGO regions). (c) and (d) AFM topographic and CAFM current mapping image corresponding to the sheet in the dashed frame in (b). The inset line profiles in (c) and (d) correspond to the dashed line and red dashed line, respectively. (e) A zoom-in current mapping of the most left rGO line in (d). The z-scale of (e) is 40 pA. (f) The Raman spectroscopy of rGO and GO regions of the pattern.

materials essentially originates from the percentage of the C=C sp^2 conjugated system, the relatively high $P_{C=C}$ indicates a recovery of electrical conductivity, as will be confirmed by the CAFM measurement later. An electrically contacted patterned sheet was located by optical microscopy as shown in the dashed frame in Figure 3(b). The corresponding topography and current mapping are shown in Figures 3(c) and 3(d). The thickness of the sheet was ca. 1 nm from the line profile analysis, which corresponded to a single layer.[21] The current mapping on SiO_2 and GO region showed no detectable difference, which indicated that the GO region was an insulator. A further precise measurement to distinguish the difference between SiO_2 and GO regions is beyond the instrument's capability. Comparatively, the rGO region was electrically conductive. From the line profile analysis of the current mapping, the current in the rGO region was obviously enhanced compared with that in the GO region. In a close-up current mapping as shown in Figure 3(e), low-conductivity domains were observed in the rGO region. The diameter of the low-conductivity domains ranged from several hundred nanometers to several micrometers. Compared with the low-conductivity domains appearing in the rGO_{64} sheet (Figure 2(e)), those in the patterned rGO/GO sheet had a larger size and a lower electrical conductivity (nearly insulating). These domains occupy a great part of the whole width of the patterned lines, which reduced the pathway of the current flowing and hence affected the electrical conductivity.

Raman spectra of the rGO region and the GO region are shown in Figure 3(f). The peaks at 1340 cm^{-1} and 1574 cm^{-1} can be ascribed to the D band and G band, respectively.[22] The intensity ratio of the D band and the G band, $I(D)/I(G)$, are always utilized to estimate the size of the graphitic and defective domains. Here, we applied the following equation to estimate the average inter-defect distance L_D:[22]

$$L_D^2(\mathrm{nm}^2) = \frac{4.3 \times 10^3}{E_L^4(\mathrm{eV}^4)} \left[\frac{I(D)}{I(G)}\right]^{-1}. \quad (2)$$

The $I(D)/I(G)$s for GO and rGO were similar and gave the value of 1.07. Hence, by using Eq. (2), the L_D was estimated to be 11.7 nm. It is interesting that the domain size observed by CAFM (Figures 2(e) and 3(e)) are larger than the theoretical value calculated from the Raman spectra here and the direct observation by STM and TEM.[1–3] Indeed, based on the XPS results, the prepared rGO_{64} actually had a similar amount of OFG residues compared with other kinds of rGO reported in some previous articles.[2,6] Therefore, the remaining OFG residues should not be the reason for the relatively larger low-conductivity domains. We believed that both the globally measured Raman results and the atomically observed microscopic results by STM[2] and TEM[3] precisely described the atomic structure of GO and rGO, where the defective domains (including both OFGs domains and sp^3 domains) were no larger than 100 nm. We propose a reasonable origin of the different conductivity between low- and high- conductivity domains as follows. Because the methods mentioned above are not capable of showing the defective domain distributions at micrometer scale, the low- and high-conductivity domains observed by CAFM are possibly hybrids of both defective domains and graphitic domains, whose ratios determine the electrical conductivity. That also explains why even the low-conductivity domains show electrical conductivity to some degree instead of being totally insulating. Further research is needed in order to address these points.

In conclusion, we have demonstrated CAFM characterization of the electrical conductivity of VUV-rGO and patterned rGO/GO sheets. By combining XPS and CAFM measurements, reduction of GO by VUV light irradiation proved to be effective and the reduced GO showed obvious enhancement of electrical conductivity. CAFM also revealed that low- and high-conductivity domains were distributed in the rGO sheet plane. The low-conductivity domains that contain residual OFGs and sp^3 carbon domains could limit further enhancement of the electrical conductivity. Nonetheless, VUV-rGO has a potential to be applied as transparent electrodes in the display and the solar cell.[23,24] The patterning capability of this photochemical process is also attractive for further applications in GO- and rGO-based electronics. The multi-exposure process combined with gas-assisted doping process of VUV light can locally define the regions of different electronic properties in a single GO layer. By this method, it can construct a single device and even integrated circuits in one graphene sheet.

[1]L. G. Cançado, A. Jorio, E. H. M. Ferreira, F. Stavale, C. A. Achete, R. B. Capaz, M. V. O. Moutinho, A. Lombardo, T. S. Kulmala, and A. C. Ferrari, Nano Lett. **11**, 3190 (2011).
[2]J. I. Paredes, S. Villar-Rodil, P. Solís-Fernández, A. Martínez-Alonso, and J. M. D. Tascón, Langmuir **25**, 5957 (2009).
[3]C. Gómez-Navarro, J. C. Meyer, R. S. Sundaram, A. Chuvilin, S. Kurasch, M. Burghard, K. Kern, and U. Kaiser, Nano Lett. **10**, 1144 (2010).
[4]S. Pei and H.-M. Cheng, Carbon **50**, 3210 (2012).
[5]D. Pandey, R. Reifenberger, and R. Piner, Surf. Sci. **602**, 1607 (2008).
[6]D. D. Kulkarni, S. Kim, M. Chyasnavichyus, K. Hu, A. G. Fedorov, and V. V. Tsukruk, J. Am. Chem. Soc. **136**, 6546 (2014).
[7]H. Dai, E. W. Wong, and C. M. Lieber, Science **272**, 523 (1996).
[8]G. Cheng, S. Wang, K. Cheng, X. Jiang, L. Wang, L. Li, Z. Du, and G. Zou, Appl. Phys. Lett. **92**, 223116 (2008).
[9]I. Tanaka, I. Kamiya, H. Sakaki, N. Qureshi, S. J. Allen, and P. M. Petroff, Appl. Phys. Lett. **74**, 844 (1999).
[10]R. L. McCreery, Chem. Mater. **16**, 4477 (2004).
[11]T. Ishida, W. Mizutani, Y. Aya, H. Ogiso, S. Sasaki, and H. Tokumoto, J. Phys. Chem. B **106**, 5886 (2002).
[12]J. M. Mativetsky, E. Treossi, E. Orgiu, M. Melucci, G. P. Veronese, P. Samorì, V. Palermo, P. Samorì, and V. Palermo, J. Am. Chem. Soc. **132**, 14130 (2010).
[13]Y. Matsumoto, M. Koinuma, S. Y. Kim, Y. Watanabe, T. Taniguchi, K. Hatakeyama, H. Tateishi, and S. Ida, ACS Appl. Mater. Interfaces **2**, 3461 (2010).
[14]Y. Tu, T. Ichii, O. P. Khatri, and H. Sugimura, Appl. Phys. Express **7**, 075101 (2014).
[15]J. Yang, T. Ichii, K. Murase, H. Sugimura, T. Kondo, and H. Masuda, Chem. Lett. **41**, 392 (2012).
[16]M. Hirata, T. Gotou, S. Horiuchi, M. Fujiwara, and M. Ohba, Carbon **42**, 2929 (2004).
[17]C. C. Teng, C. C. M. Ma, C. H. Lu, S. Y. Yang, S. H. Lee, M. C. Hsiao, M. Y. Yen, K. C. Chiou, and T. M. Lee, Carbon **49**, 5107 (2011).
[18]P. Blake, E. W. Hill, A. H. Castro Neto, K. S. Novoselov, D. Jiang, R. Yang, T. J. Booth, A. K. Geim, A. H. C. Neto, K. S. Novoselov, D. Jiang, R. Yang, T. J. Booth, and A. K. Geim, Appl. Phys. Lett. **91**, 63124 (2007).
[19]Y. Zhou, Q. Bao, B. Varghese, L. A. L. Tang, C. K. Tan, C. H. Sow, and K. P. Loh, Adv. Mater. **22**, 67 (2010).
[20]Y. Zhang, L. Guo, S. Wei, Y. He, H. Xia, Q. Chen, H. B. Sun, and F. S. Xiao, Nano Today **5**, 15 (2010).
[21]C. Gómez-Navarro, R. T. Weitz, A. M. Bittner, M. Scolari, A. Mews, M. Burghard, and K. Kern, Nano Lett. **7**, 3499 (2007).
[22]A. C. Ferrari and D. M. Basko, Nat. Nanotechnol. **8**, 235 (2013).
[23]G. Eda and M. Chhowalla, Adv. Mater. **22**, 2392 (2010).
[24]Z. Yin, S. Sun, T. Salim, S. Wu, X. Huang, Q. He, Y. M. Lam, and H. Zhang, ACS Nano **4**, 5263 (2010).